Available online at www.sciencedirect.com
SCIENCE DIRECT
Thin Solid Films 506–507 (2006) 454 – 459
thin solid films
www.elsevier.com/locate/tsf

Two-dimensional calculation of spatial distribution of neutral atoms for a planar inductively coupled oxygen discharge

H.J. Yoon [a], T.H. Chung [a,*], C.J. Chung [a], J.K. Lee [b]

[a] Department of Physics, Dong-A University, Busan 604-714, Korea
[b] Department of Electronic and Electrical Engineering, Pohang University of Science and Technology, Pohang 790-784, Korea

Available online 15 September 2005

Abstract

Two-dimensional self-consistent fluid simulation of inductively coupled oxygen plasma is presented. The model equations include continuity equations for charged species and neutral oxygen atom, the Poisson equation, and the electron energy balance equation. The drift–diffusion approximation is employed. From the Maxwell equations, the induced electric field and absorbed power are calculated. The two-dimensional spatial distributions of charged species densities, charged species flux, density and flux of atomic oxygen, electric potential, and electron temperature are calculated. The effect of the gas pressure on the plasma uniformity is investigated. As the pressure increases, the spatial distributions of charged species and neutral atom have their peak values in the toroidal region where a large amount of the input power is absorbed by the plasma.

Keywords: Oxygen discharge; Fluid simulation; Plasma uniformity

1. Introduction

Plasma processing utilizes chemically reactive discharges in order to etch or deposit material onto substrates of interest. The uniformity of radicals or neutral atoms on the wafer has been an important issue in the plasma processing utilizing high-density plasma sources. Thus, the mechanisms that determine the uniformity of chemically reactive neutrals are of interest. Process uniformity depends strongly on the spatial distribution of both charged and neutral particle densities and velocities, as well as potentials [1,2]. Process uniformity is a key requirement to enable large wafers or flat panels to be processed by plasma.

In this study, an oxygen plasma is considered since it has found numerous applications in plasma processing, such as plasma enhanced chemical vapor deposition, reactive sputtering, dry etching of polymers, oxidation, and resist removal of semiconductors. Especially spatial distributions of density and flux of atomic oxygen are studied since atomic oxygen plays an important role in various plasma processes like surface modification of synthetics, surface cleaning, growth of silicon oxide films, and etching [1,3,4].

Two-dimensional self-consistent fluid simulation of inductively coupled oxygen plasma with a one-turn antenna placed on the top of the dielectric roof is presented. In a previous study [5], we performed similar calculations for inductively coupled oxygen discharge. However, that study was based on consideration of three species in the plasma (O_2^+, O^- and electron) and did not include the equations for the oxygen atom and O^+. Etch rates and the shape of etched profiles depend on the relative flux of O_2, O, O_2^+, and O^+. The transition from an O_2 to O-dominated plasma is smooth, with almost no O_2 dissociated in the capacitive mode, and a gradual increase in percent dissociation with increasing power in the inductive mode. The fractional densities of O^+ and O_2^+ influence both plasma steady state conditions and plasma surface interaction during etching.

Numerical modeling of plasma generation and transport can be useful for improving our understanding of high-density oxygen plasmas and for investigating the effect of reactor design and operating conditions on plasma uniformity over semiconductor wafers.

* Corresponding author. Tel.: +82 51 200 7228; fax: +82 51 200 7232.
E-mail address: thchung@plasma.donga.ac.kr (T.H. Chung).

0040-6090/$ - see front matter © 2005 Elsevier B.V. All rights reserved.
doi:10.1016/j.tsf.2005.08.044

2. Model equations

The model equations include continuity equations for charged species and neutral oxygen atom, the Poisson equation, and the electron energy balance equation. The drift–diffusion approximation is employed. From the field solver using full Maxwell equations, the induced electric field and absorbed power are calculated. The reactions in high-density oxygen discharges considered in this model are described in Table 1. It should be noted that reactions with O^+ are considered because efficient production of O^+ is realized in high-density oxygen discharges [6]. Metastable excited state of $O_2(a^1\Delta_g)$ is neglected for simplicity of the model. The effect of $O_2(a^1\Delta_g)$ is not significant for the low pressure and moderate power region considered in this study [7]. The rate coefficients are adopted from Ref. [7]. The spatial profiles of densities of charged species and neutral oxygen depend on the reaction rates of the constituents. Ion–ion recombination is assumed to be the dominant loss mechanism for high density oxygen discharges.

The species conservation equations are given by

$$\frac{\partial n_j}{\partial t} + \nabla\cdot\boldsymbol{\Gamma_j} = \sum_i R_{ij}. \tag{1}$$

Here n_j is the density of species j (=O, O_2^+, O^+, e), $\boldsymbol{\Gamma_j}$ is the flux of species j, and R_{ij} is the rate of production or consumption of species j from homogeneous reactions of the type i. To our best knowledge, the equations for O^+ and O species have not been included in other researcher's previous works for the fluid simulation of inductively coupled oxygen plasmas. Instead of solving the momentum balance equation, the drift–diffusion approximation is used for particle flux

$$\boldsymbol{\Gamma_j} = -D_j\nabla n_j \pm n_j\mu_j\mathbf{E}. \tag{2}$$

The energy balance equation is written as

$$\frac{\partial}{\partial t}\left(\frac{3}{2}n_e kT_e\right) + \nabla\cdot\mathbf{q_e} + e\boldsymbol{\Gamma_e}\cdot\mathbf{E} + \sum_l H_l R_l = P_{\text{abs}}. \tag{3}$$

The heat flux vector is

$$\mathbf{q_e} = -\frac{5}{2}n_e D_e\nabla(kT_e) + \frac{5}{2}kT_e\boldsymbol{\Gamma_e}. \tag{4}$$

Poisson's equation is expressed as

$$\nabla^2 V = -\frac{1}{\epsilon_0}\sum_j q_j n_j. \tag{5}$$

Here D_j and μ_j are the diffusion coefficient and mobility of species j and V, T_e, k, e, ϵ_0 are potential, electron temperature, Boltzmann constant, electron charge and permittivity of free space, respectively. H_l is the electron energy loss per collision. Boundary conditions are $V=0$, $n_j=0$, and $\nabla T_e=0$ at grounded cylinder wall.

The absorbed power P_{abs} is obtained by solving Maxwell's equation. For an axisymmetric external current, J_{ext}, we obtain the induced electric field in the vacuum

$$\nabla^2\tilde{E}_\theta(r,z) + \frac{\omega^2}{c^2}\tilde{E}_\theta(r,z) = -i\omega\mu_0 J_{\text{ext}} \tag{6}$$

Then, this field is inserted as a source term of the Maxwell's equation for finding the induced electric field in the plasma

$$\nabla^2 E_\theta(r,z) + \frac{\omega^2}{c^2}E_\theta(r,z) = i\omega\mu_0\sigma(r,z)\tilde{E}_\theta, \tag{7}$$

where $\sigma(r,z)$ is the cold plasma conductivity, and μ_0 is the permeability of free space. The spatial profile of energy

Table 1
Model reaction set for an oxygen plasma

Reactions		Rate coefficients	Units
Ionization 2	$e+O_2\rightarrow O_2^+ + 2e$	$K_{iz2} = 9.0\times10^{-16}T_e^2\exp\left(-\frac{12.6}{T_e}\right)$	$m^3\ s^{-1}$
Dissociative attachment	$e+O_2\rightarrow O^- + O$	$K_{att} = 8.8\times10^{-17}\exp\left(-\frac{4.4}{T_e}\right)$	$m^3\ s^{-1}$
Recombination 2	$O_2^+ + O^-\rightarrow O_2 + O$	$K_{rec2} = 1.5\times10^{-13}\left(\frac{300}{T_g}\right)^{0.5}$	$m^3\ s^{-1}$
Recombination 1	$O^- + O^+\rightarrow O + O$	$K_{rec1} = 2.5\times10^{-13}\left(\frac{300}{T_g}\right)^{0.5}$	$m^3\ s^{-1}$
Detachment	$e+O^-\rightarrow O+2e$	$K_{det} = 2.0\times10^{-13}\exp\left(-\frac{5.5}{T_e}\right)$	$m^3\ s^{-1}$
Dissociative ionization	$e+O_2\rightarrow O+O^+ +2e$	$K_{disiz} = 5.3\times10^{-16}T_e^{0.9}\exp\left(-\frac{20}{T_e}\right)$	$m^3\ s^{-1}$
Ionization 1	$e+O\rightarrow O^+ +2e$	$K_{iz1} = 9.0\times10^{-15}T_e^{0.7}\exp\left(-\frac{13.6}{T_e}\right)$	$m^3\ s^{-1}$
Dissociation	$e+O_2\rightarrow 2O+e$	$K_{diss} = 4.2\times10^{-15}\exp\left(-\frac{5.6}{T_e}\right)$	$m^3\ s^{-1}$

deposition rate to the electrons is the time average over the wave period,

$$P_{\text{abs}} = Re\left(\sigma|E_\theta(r, z)|^2\right). \quad (8)$$

In this study, a model of the collisionless electron heating is not considered. The effects of the collisionless electron heating can be incorporated into the conductivity term in Eq. (8) by introducing the effective collision frequency which includes the stochastic heating. The charged particles flux and the flux of electron energy are obtained by the method of exponential scheme [8]. The equations are discretized by the finite difference method for the spatial derivatives, while the time derivatives are discretized by the forward Euler differencing (FTCS). The details of the numerical method are in Ref. [9].

3. Results and discussion

We consider a cylinder with a planar single-turn loop antenna. The cylinder chamber has dimensions of 35 cm height and 17 cm radius. The quartz window of the thickness 2 cm is inside the chamber. The antenna is located at $r = 10$ cm from the axis. The plasma volume is a cylinder of 17 cm radius and 28 cm height (from the location of quartz window to the bottom of the cylinder) without a substrate plate. Fig. 1 shows the two-dimensional distributions of the electric potential, electron temperature, electron density, negative ion density, and positive ion densities. The electron temperature has a spatially uniform distribution in the bulk region, and almost symmetric in both sheaths. It is further observed that the charged particle density is rather uniform in the radial direction. The electron density decreases smoothly toward the radial sheath, whereas the negative ion density has a quite drastic drop near the radial sheath. As can be seen in Fig. 1, the density profiles of negative ions have more steep slopes than those of positive ions along the distance. In other words, the profiles of negative ions show stronger density gradients to the wall than those of positive ions. Moreover, in the bulk region, quasi-neutrality is achieved. Although not shown in the figure, the inductive electric field and thus the absorbed power peak at 8 cm from the center axis and 3 cm below the quartz window.

Fig. 2 shows the density profiles of the positive ions at various pressures. The calculated density profiles are somewhat flatter for lower gas pressures. At higher pressures, the ratio of ion production or depletion rates (ionization, ion–ion recombination, and attachment) to the diffusion rates of positive or negative ion becomes larger. Positive and negative ions are either produced or depleted much faster than they are diffused; large concentration gradients then develop [10]. The plasma uniformity has been observed to degrade at higher pressure [4].

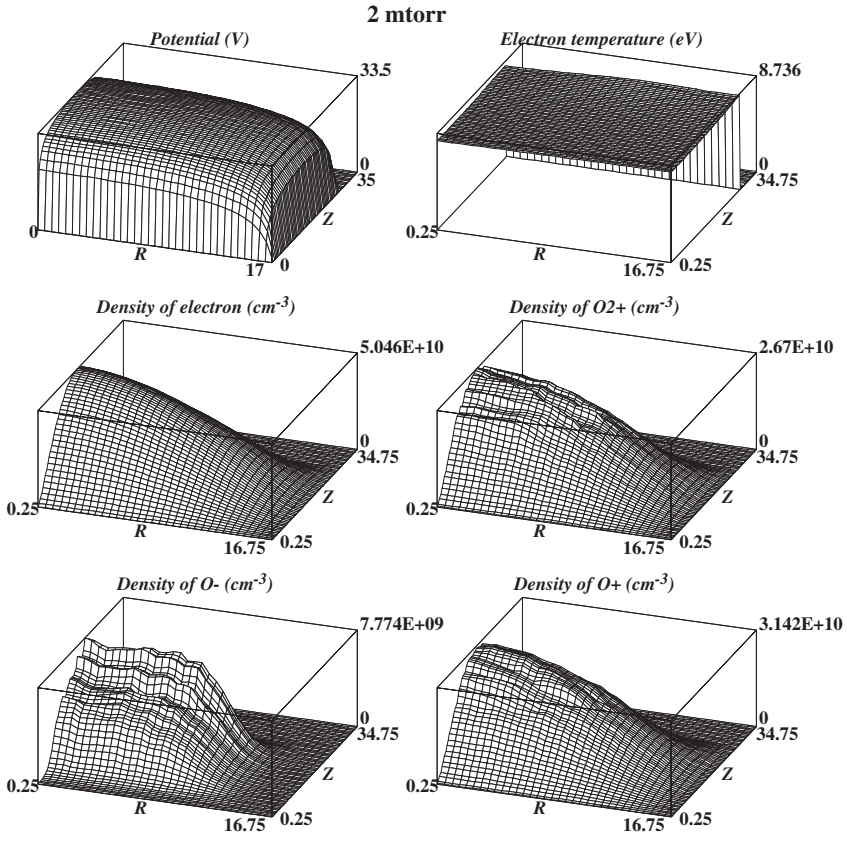

Fig. 1. The spatial profiles of potential, electron temperature, electron density, negative ion density, positive ion densities where $P_{\text{rf}} = 100$ W, $p = 2$ mTorr.

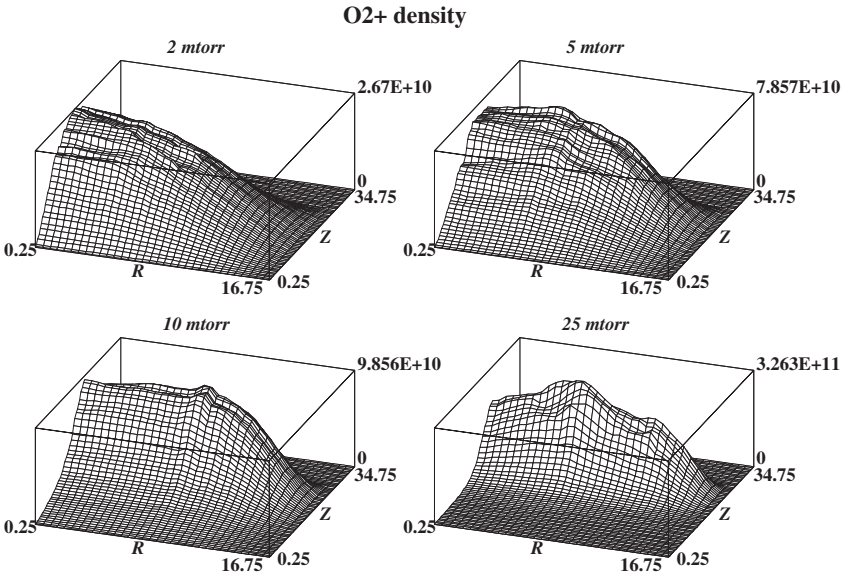

Fig. 2. Density profiles of positive ions at various pressures (p=2, 5, 10, 25 mTorr) where P_{rf}=100 W.

Fig. 3 shows the density profiles of the neutral O atoms at various pressures. We expect a significant depletion of neutral atom density due to both ionization and plasma collisional heating. As the pressure increases, the spatial distributions of charged species and neutral atom have their peak values in the toroidal region where a large amount of the input power is absorbed by the plasma through the one-turn antenna. In Fig. 3, we can observe that the profile of oxygen atoms is peaked in the center at pressures of 2, 5 and 10 mTorr, in contrast to that of the argon discharge. In the case of monatomic gas, the feed neutral gas itself experiences rapid depletion (ion-pumping effect). Because this removal rate is much faster than the rate of thermal neutral diffusion from the walls or gas injection sources, the neutral density in the central portion of the plasma can be significantly reduced [4,11]. The neutral atom in an oxygen discharge has a behavior different from that in the monatomic feed gas case like argon. The calculated radial distributions of oxygen atoms are in agreement with the experimental results [1,4]. The profile of oxygen atom is parabolic (peaked in the plasma center) or hollow, depending on the gas pressure. Overall, the uniformity of oxygen atoms becomes worse as the pressure increases. In a microwave oxygen discharge, the atomic oxygen homogeneity is observed to degrade with increasing pressure [12]. At a lower pressure, the oxygen atom density is nearly

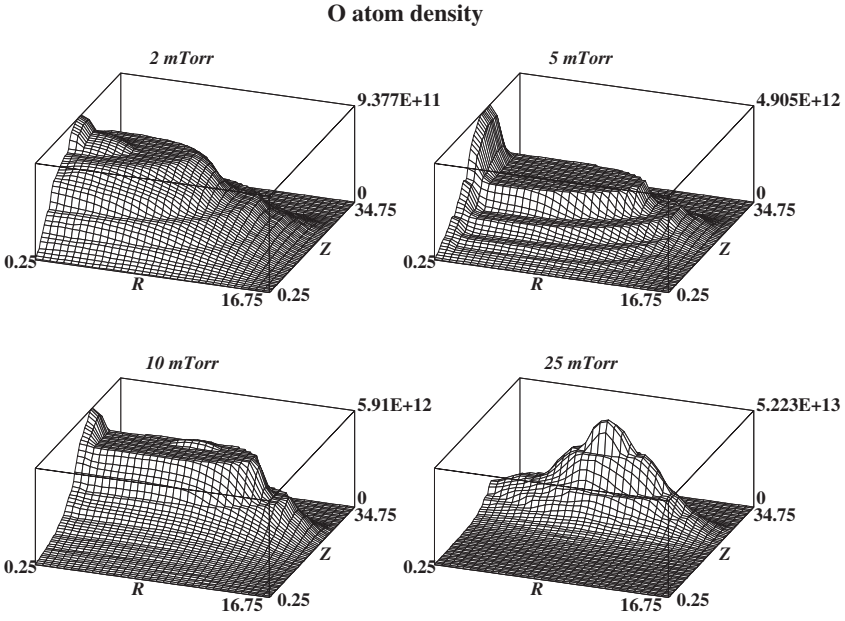

Fig. 3. Density profiles of oxygen atoms at various pressures (p=2, 5, 10, 25 mTorr) where P_{rf}=100 W.

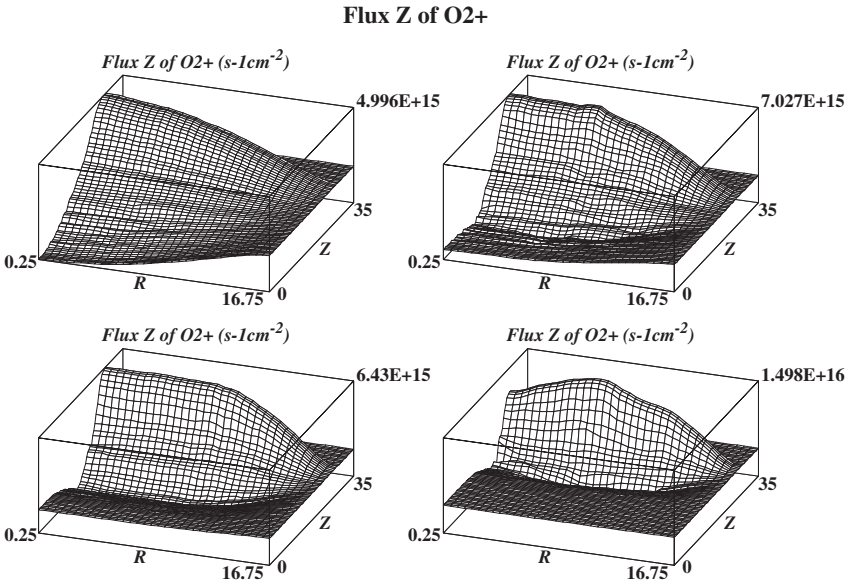

Fig. 4. Spatial profiles of O_2^+ flux in the z-direction at various pressures (p=2, 5, 10, 25 mTorr) where P_{rf}=100 W.

homogeneous due to the greater diffusion length [12]. The calculated profile of oxygen atoms compares well with the relative radial distribution of the F density which was obtained by optical emission actinometry in SF_6 discharges [13] and CF_4 discharges [14]. The variation of the magnitude of the spatially averaged density of oxygen atoms with operating pressure was predicted by global modeling [15]. The oxygen atom density increases with pressure in the low-pressure range, and this was observed experimentally in an inductively coupled plasma [16] and a microwave discharge [3].

Fig. 4 shows the spatial profiles of O_2^+ flux in the z-direction (which is normal to the substrate surface). Since we have not considered the substrate (power, geometry, and rf frequency), the flux in this case means the vector quantity of fluid velocity multiplied by the particle density. From the figures, we can notice that the substrate should be placed adjacent to the plasma generation region in order to have a substantial amount of positive ion flux. The radial uniformity of the incident flux seems good, but the flux uniformity in z-direction becomes worse as the pressure increases.

The Langmuir probe measurement of positive ion densities is performed in the radial direction of the chamber and the normalized density profiles are compared with the calculated values in Fig. 5. The values calculated by the

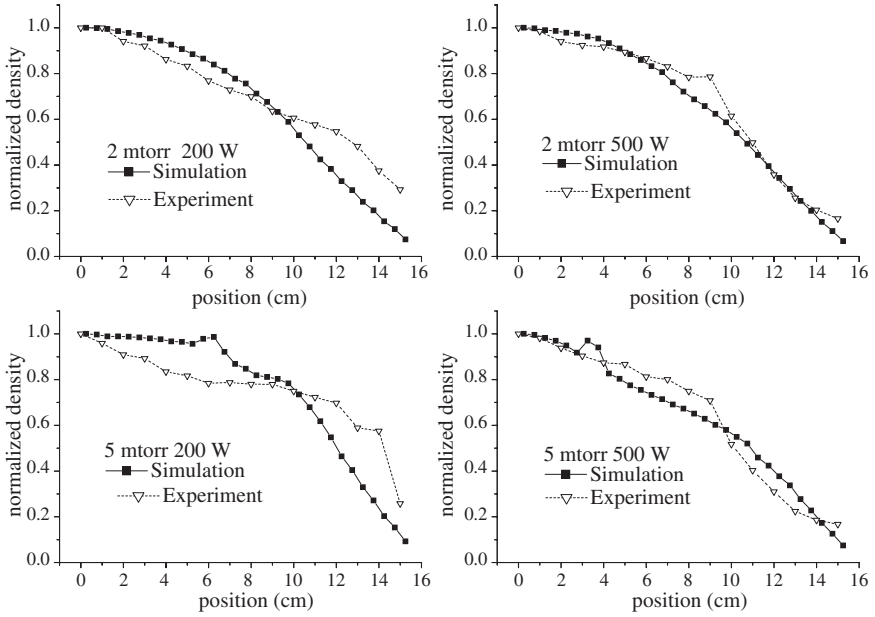

Fig. 5. Comparison of radial distributions of positive ion density between the calculation and the Langmuir probe measurement at various pressures and powers (p=2, 5 mTorr, P_{rf}=200, 500 W).

fluid modeling are higher than the experimental values. The reason for this is that, since the supplied rf power is partly reflected and dissipated in the circuit and antenna, the actual absorbed power is less than the input power of the power supply. In addition, there are many losses of energy associated with the various species, which are not considered by the numerical model. The details of the Langmuir probe measurement are found in Ref. [17]. Overall, they agree. Especially, a good agreement is achieved for a lower pressure, higher power case (2 mTorr, 500 W).

4. Conclusion

The two-dimensional fluid simulation of inductively coupled oxygen plasma is performed. The numerical model includes the equations for O^+ and O, which has not been investigated previously. The equilibrium two-dimensional profiles of charged species and neutral atoms of high-density oxygen discharges are numerically calculated. The negative and positive ion concentrations in the bulk are assumed to be mostly determined by ionization, attachment, and recombination reactions. The simulation results compare well with experiments. The calculated density profiles are somewhat flatter for lower gas pressures. At higher pressures, the ratio of ion production or depletion rates to the diffusion rates of positive or negative ions becomes larger. Positive and negative ions are produced or depleted much faster than they are diffused; hence, large concentration gradients then develop. The plasma uniformity is observed to degrade at higher pressure. The profile of oxygen atoms is parabolic (peaked in the plasma center) or hollow (in a strict manner, humped), depending on the gas pressure. A model of collisionless electron heating for low pressure discharge operation should be included in a subsequent study. Optical emission actinometry experiments are being performed to confirm the validity of this model.

Acknowledgments

This work is supported by the Research Fund of Dong-A University (the program year of 2004).

References

[1] S. Yun, G.R. Tynan, J. Appl. Phys. 89 (2001) 911.
[2] T. Hori, M.D. Bowden, K. Uchino, K. Muraoka, J. Vac. Sci. Technol., A 14 (1996) 144.
[3] M. Naddaf, V.N. Bhoraskar, A.B. Mandale, S.R. Sainkar, Plasma Sources Sci. Technol. 11 (2002) 361.
[4] S. Yun, K. Taylor, G.R. Tynan, Phys. Plasmas 7 (2000) 3448.
[5] H.J. Yoon, T.H. Chung, D.C. Seo, Jpn. J. Appl. Phys. 38 (1999) 6890.
[6] T. Mieno, K. Kamo, D. Hayashi, T. Shoji, K. Kadota, Appl. Phys. Lett. 69 (1996) 617.
[7] J.T. Gudmundsson, I.G. Kouznetsov, K.K. Patel, M.A. Lieberman, J. Phys. D: Appl. Phys. 34 (2001) 1100.
[8] D.L. Sharfetter, H.K. Gummel, IEEE Trans. Electron Devices 16 (1969) 64.
[9] J.K. Lee, L. Meng, Y.K. Shin, H.J. Lee, T.H. Chung, Jpn. J. Appl. Phys. 36 (1997) 5714.
[10] T.W. Kim, E.S. Aydil, IEEE Trans. Plasma Sci. 31 (2003) 614.
[11] M. Yoon, S.C. Kim, H.J. Lee, J.K. Lee, J. Korean Phys. Soc. 32 (1998) L635.
[12] St. Behle, A. Georg, Y. Yuan, J. Engemann, A. Brockhaus, Surf. Coat. Technol. 97 (1997) 734.
[13] P.W. Lee, Y.J. Kim, C.S. Chang, H.Y. Chang, Rev. Sci. Instrum. 66 (1995) 4591.
[14] M. Sarfaty, M. Harper, N. Hershkowitz, Rev. Sci. Instrum. 69 (1998) 3176.
[15] H.J. Yoon, T.H. Chung, J. Korean Phys. Soc. 39 (2001) 271.
[16] D.C. Seo, T.H. Chung, J. Phys. D: Appl. Phys. 34 (2001) 2854.
[17] D.C. Seo, T.H. Chung, H.J. Yoon, G.H. Kim, J. Appl. Phys. 89 (2001) 4218.